MOLECULAR AND CELLULAR BIOLOGY, Aug. 2005, p. 6980–6989 Vol. 25, No. 16
0270-7306/05/$08.00+0 doi:10.1128/MCB.25.16.6980–6989.2005

Increased Vascular Smooth Muscle Contractility in *TRPC6*$^{-/-}$ Mice

Alexander Dietrich,[1] Michael Mederos y Schnitzler,[1] Maik Gollasch,[2]† Volkmar Gross,[2] Ursula Storch,[1] Galyna Dubrovska,[2] Michael Obst,[2] Eda Yildirim,[3] Birgit Salanova,[2] Hermann Kalwa,[1] Kirill Essin,[2] Olaf Pinkenburg,[1] Friedrich C. Luft,[2] Thomas Gudermann,[1]* and Lutz Birnbaumer[3]

Institut für Pharmakologie und Toxikologie, Philipps-Universität Marburg, Marburg, Germany[1]; Franz-Volhard Klinik, HELIOS Klinikum-Berlin, Medizinische Fakultät der Charité, Max-Delbrück-Centrum, Berlin, Germany[2]; and National Institute of Environmental Health Sciences, Research Triangle Park, North Carolina 27709[3]

Received 17 February 2005/Returned for modification 24 March 2005/Accepted 29 May 2005

Among the TRPC subfamily of TRP (classical transient receptor potential) channels, TRPC3, -6, and -7 are gated by signal transduction pathways that activate C-type phospholipases as well as by direct exposure to diacylglycerols. Since TRPC6 is highly expressed in pulmonary and vascular smooth muscle cells, it represents a likely molecular candidate for receptor-operated cation entry. To define the physiological role of TRPC6, we have developed a TRPC6-deficient mouse model. These mice showed an elevated blood pressure and enhanced agonist-induced contractility of isolated aortic rings as well as cerebral arteries. Smooth muscle cells of TRPC6-deficient mice have higher basal cation entry, increased TRPC-carried cation currents, and more depolarized membrane potentials. This higher basal cation entry, however, was completely abolished by the expression of a TRPC3-specific small interference RNA in primary *TRPC6*$^{-/-}$ smooth muscle cells. Along these lines, the expression of TRPC3 in wild-type cells resulted in increased basal activity, while TRPC6 expression in *TRPC6*$^{-/-}$ smooth muscle cells reduced basal cation influx. These findings imply that constitutively active TRPC3-type channels, which are up-regulated in TRPC6-deficient smooth muscle cells, are not able to functionally replace TRPC6. Thus, TRPC6 has distinct nonredundant roles in the control of vascular smooth muscle tone.

The TRP (transient receptor potential) family of ion channels is a growing group of structurally and evolutionarily related cation channels formed of several subfamilies that include the TRPC, TRPM, and TRPV classes of channels (6, 22). TRP-type ion channels are presumed to be homo- or heterotetramers (13, 14), each spanning the plasma membrane six times. The founding members of this channel family are the insect TRP and TRPL channels, which are responsible for photoreceptor depolarization in response to light. Mammalian TRPCs (C stands for canonical or classical) (23, 32) are the closest mammalian structural relatives of insect TRPs. Among the TRPC channels, TRPC3, -6, and -7 are 75% identical and gated by signal transduction pathways that activate C-type phospholipases (3, 32) as well as by direct exposure to diacylglycerols (DAG) (15). TRPC3, -6, and -7 interact physically and, upon coexpression, coassemble to form functional channels (14). Expression of TRPC3 and TRPC7 in HEK 293 cells, but not of TRPC6, reveals constitutively active cation channels that are permeable not only to monovalent but also to divalent cations such as Ca^{2+}, Ba^{2+}, and Mn^{2+} (7, 23, 33).

In contrast to members of other TRP families, the functional importance of most members of the TRPC subfamily is still poorly understood. A TRPC channel for which considerable evidence has accumulated for a specific role is TRPC6, which has been proposed to regulate smooth muscle function. The TRPC6 mRNA was originally isolated from mouse brain and was also identified in lung cells (4). By comparative biophysical characterization and gene suppression using antisense oligonucleotides, TRPC6 was suggested to be the molecular correlate of the α_1-adrenoceptor-activated nonselective cation channel in vascular smooth muscle cells (16) and the vasopressin-activated cation channel in an aortic smooth muscle cell line (18). In addition, TRPC6 has been proposed to play a critical role in the intravascular pressure-induced depolarization and constriction of small arteries and arterioles in the brain (29). Activation of nonselective cation channels in vascular smooth muscle cells subsequent to receptor activation leads to cation influx and depolarization followed by the recruitment of voltage-gated L-type Ca^{2+} channels, which mediate the bulk of the Ca^{2+} influx, resulting in smooth muscle contraction (reviewed in reference 12). The experimental studies just mentioned (16, 18, 29) strongly support the notion that TRPC6 is an essential component of receptor-operated Ca^{2+}-permeable nonselective cation channels in smooth muscle cells.

We have developed mice deficient in TRPC6, and based on the data reviewed above, we predicted that loss of TRPC6 function would lead to a loss of vascular smooth muscle tone and attendant hypotension. Unexpectedly, we observed a higher agonist-induced contractility in isolated aortic rings prepared from these mice and an elevated systemic blood pressure that was further increased by inhibition of nitric oxide syn-

* Corresponding author. Mailing address: Institut für Pharmakologie und Toxikologie, Philipps-Universität Marburg, Karl-von-Frisch-Str. 1, 35043 Marburg, Germany, Phone: 49 6421 2865000. Fax: 49 6421 2865600. E-mail: guderman@staff.uni-marburg.de.

† Present address: Medizinische Klinik mit Schwerpunkt Nephrologie und internistische Intensivmedizin, Charité Campus Virchow Klinikum, Berlin, Germany.

thase. These effects were brought about by in vivo replacement of TRPC6 by channels of the TRPC3 type, a closely related but constitutively active member of the DAG-activated TRPC3/6/7 family. This resulted in enhanced basal and agonist-induced cation entry into smooth muscle cells, leading to more depolarized membrane potentials and increased smooth muscle contractility. The higher basal cation entry, however, was completely abolished by the expression of a TRPC3-specific small interference RNA (siRNA) in primary *TRPC6*$^{-/-}$ smooth muscle cells.

To summarize, we provide in vivo and in vitro evidence that TRPC3 and TRPC6 are not freely functionally interchangeable. Thus, TRPC6 plays a cardinal role in receptor-operated control of vascular smooth muscle tone and has distinct and nonredundant roles in whole-animal vascular smooth muscle physiology.

MATERIALS AND METHODS

Targeting vector construction, gene disruption, and genotyping of TRPC6-deficient mice. The targeting vector was designed to replace exon 7 of the mouse TRPC6 gene and was constructed using genomic DNA fragments from a 129Sv genomic library cloned into P1 phages (Genome Systems, Berkeley, Calif.). The library was screened with primers specific for the genomic mouse TRPC6 sequence (32).

After linearization, the vector was used to target EK-CCE embryonic stem (ES) cells as described previously (17). A heterozygous ES clone (48F) was identified by Southern blotting. This clone was devoid of vector (pBS) or phosphoglycerate kinase (PGK)-Neo DNA elsewhere in the genome and showed integration of the PGK-Neo sequence at the correct site as shown by screening with both the 5′ external probe and the Neo probe. Germ line chimeras were obtained by injection of the correctly targeted ES cell clone 48F into C57BL/6J blastocysts and crossed to homozygosity in a 1:1 129Sv:C57BL/6J background.

Offspring were analyzed by PCR using as template the genomic DNA extracted from mouse tail biopsy samples and the forward and reverse primer pair C6-E7F and C6-E7R, which annealed to exon 7 of the TRPC6 gene for wild-type (WT) detection, and primer pair C6-IFF and PgkR, which annealed to the intron downstream of exon 7 of the *TRPC6* gene and the PGK promoter of the disrupting PGK-Neo cassette for mutant detection. Predicted reaction products were 234 bp for the wild type and 339 bp for the mutated genotypes. Primer sequences were as follows: C6-E7F, 5′-CAG ATC ATC TCT GAA GGT CTT TAT GC; C6-E7R, 5′-TGT GAA TGC TTC ATT CTG TTT TGC GCC; C6-IFF, 5′-GGG TTT AAT GTC TGT ATC ACT AAA GCC TCC; PgkR, 5′-ACG AGA CTA GTG AGA CGT GCT ACT TCC.

Only 129Sv/C57BL/6J littermates (WT, TRPC6$^{-/-}$, or TRPC6$^{+/-}$) were analyzed. All experiments involving animals were approved by the local council on animal care.

Reverse transcription-PCR (RT-PCR) and Western blot analysis. Total RNA from lung cells was isolated using the TriFast reagent (PeqLab, Erlangen, Germany). First-strand synthesis was carried out with random hexamers (pdN_6; Amersham Bioscience, Freiburg, Germany) as primers, using REVERTAID reverse transcriptase (MBI-Fermentas, Sankt Leon-Roth, Germany). Products were amplified using TRPC6-specific primer pairs F1 and R1, F2 and R2, and F3 and R3, giving predicted product sizes of 456 bp, 1,172 bp, and 584 bp, respectively, and β-actin primers (ACTF and ACTR) as controls. Primer sequences were as follows: F1, 5′-GCT CCC GCT GCC ACC GTA TG; F2, 5′-ACT TCG GCC GTC CAA ATC TCA GC; F3, 5′-TCT GGG CTA TCT TTG GTC TTT CTG; R1, 5′-CTG GGG CTT GTC GCT AAC CTT TTG; R2, 5′-GGC CCT TGC AAA CTT CCA CTC CA; R3, 5′-ATC AAT CTG GGC CTG CAA TAC ATA; ACTF, 5′-GGC TAC AGC TTC ACC ACC AC; ACTR, 5′-GAG TAC TTG CGC TCA GGA GG. PCRs were carried out using the following conditions: initial denaturation for 3 min at 94°C and 45 cycles of 94°C for 30 s, 55°C for 30 s, and 72°C for 1 min, followed by a final extension at 72°C for 7 min. Western blot analysis of proteins from embryonic brain was carried out as described previously (27) using a TRPC6-specific antiserum (Alomone Labs, Jerusalem, Israel).

Contraction of arterial smooth muscle rings. Thoracic aortas were transferred to cold (4°C) oxygenated (95% O_2-5% CO_2) physiological salt solution (119 mM NaCl, 4.7 mM KCl, 25 mM $NaHCO_3$, 1.2 mM KH_2PO_4, 1.6 mM $CaCl_2$, 1.2 mM $MgSO_4$, 0.03 mM EDTA, and 11 mM glucose) and dissected into 2-mm rings as described previously (19). Arterial segments were stretched in a stepwise manner to preloads of approximately 0.8 g. Mesenteric arteries were prepared as described previously (21) and mounted into a small-vessel myograph (Danish Myotechnology, Aarhus, Denmark).

Blood pressure analysis by telemetric techniques. Experiments were performed on seven male *TRPC6*$^{-/-}$ mice weighing 26 ± 1 g and five male controls (four *TRPC6*$^{+/-}$ and one wild type) weighing 27 ± 1 g. L-NAME (*N*′-nitro-L-arginine methyl ester) treatment was performed on six *TRPC6*$^{-/-}$ mice and four controls. One mouse was lost from each group for technical reasons. Body weights of L-NAME-treated mice were stable (body weights at the end of treatment were as follows: *TRPC6*$^{-/-}$ mice, 27 g; controls, 26 g). Telemetric techniques are described in detail elsewhere (11), with the exception that the catheter of the telemetry device was advanced via the femoral artery into the abdominal aorta and the body of the transmitter was placed subcutaneously along the animal's flank. We quantified L-NAME uptake by weighing drinking bottles and calculating daily water uptake. Averaged over 5 to 7 days, the daily L-NAME uptake was 101 and 102 mg/kg of body weight/day in the case of control mice and *TRPC6*$^{-/-}$ mice, respectively.

Analysis of the myogenic tone in mouse cerebral arteries. After decapitation of mice, the brain was removed and quickly transferred to cold (4°C), oxygenated (95% O_2-5% CO_2) physiological salt solution. Arteries were mounted onto glass cannulas on both sides, allowing an application of hydrostatic pressure to the vessel as described previously (20). For calibration and details, see reference 10.

Quantitative real-time PCR. Total RNA and first-strand synthesis was carried out as described above. The following primers pairs were used for the amplification of specific fragments from the first-strand synthesis: TRPC1, C1F (5′-TGG GCC CAC TGC AGA TTT CAA) and C1R (5′-AAG ATG GCC ACG TGC GCT AAG GAG); TRPC2, C2F (5′-TTG CCT CCC TCA TCT TCC TCA CCA) and C2R (5′-CCG CAA GCC CTC GAT CCA CAC CT); TRPC3, C3F (5′-AGC CGA GCC CCT GGA AAG ACA C) and C3R (5′-CCG ATG GCG AGG AAT GGA AGA C); TRPC4, C4F (5′-GGG CGG CGT GCT GCT GAT) and C4R (5′-CCG CGT TGG CTG ACT GTA TTG TAG); TRPC5, C5F (5′-AGT CGC TCT TCT GGT CTG TCT TT) and C5R (5′-TTT GGG GCT GGG AAT AAT G); TRPC6, C6F (5′-GAC CGT TCA TGA AGT TTG TAG CAC) and C6R (5′-AGT ATT CTT TGG GGC CTT GAG TCC); TRPC7, C7F (5′-GTG GGC GTG CTG GAC CTG) and C7R (5′-AGA CTG TTG CCG TAA GCC TGA GAG); $Ca_V1.2\alpha_1$, α1CF (5′-GAC GTT CCC CCA GGC TGT GTT ACT) and α1CR (5′-GTG ATG GGG ACC GAG GAT AGA CC); and β-actin (ACTF and ACTR) primers as described above. Real-time PCR was done using the 2× master mix from the Quantitect SYBR Green PCR kit (QIAGEN, Hilden, Germany) containing a HotStar *Taq* polymerase, buffer, nucleotides, 5 mM $MgCl_2$ (final concentration, 2.5 mM), and SYBR Green. Ten picomoles of each primer pair and 0.2 μl from the first-strand synthesis were added to the reaction mixture, and PCR was carried out in a light cycler apparatus (Roche, Mannheim, Germany) using the following conditions: 15 min of initial activation and 45 cycles of 12 s at 94°C, 30 s at 50°C, 30 s at 72°C, and 10 s at 80°C each. Fluorescence intensities were recorded after the extension step at 80°C after each cycle to exclude fluorescence of primer dimers melting at temperatures lower than 80°C. All primers were tested by using diluted cDNA from the first-strand synthesis (10- to 1,000-fold) to confirm linearity of the reaction. Samples containing primer dimers were excluded by melting curve analysis and identification of the products by agarose gel electrophoresis. Crossing points were determined by the software program. The relative gene expression was quantified using the formula $[2e^{(\text{crossing point of } \beta\text{-actin} - \text{crossing point X})}] \times 100 = \%$ of reference gene expression.

Smooth muscle cell isolation and Ba^{2+} influx experiments. Thoracic aortas were placed in cold (4°C) solution I (127 mM NaCl, 5.9 mM KCl, 1.2 mM $MgCl_2$, 11.8 mM glucose, 10 mM HEPES, pH 7.4, 2.4 mM $CaCl_2$). After blood vessels were washed once in solution I without $CaCl_2$ added, aortas were cut longitudinally into two pieces and placed into solution EI containing enzymes (from Sigma-Aldrich, Deisenhofen, Germany; 5 mg of albumin per ml [A4503], 3.5 mg of papain per ml [P4762], and 5 mg of dithiothreitol per ml [43815] in Ca^{2+}-free solution I) for 30 min at 37°C. Afterwards, pieces were incubated in enzyme solution EII containing 5 mg of albumin per ml, 5 mg of collagenase per ml (C8051), and 5 mg of hyaluronidase per ml (H3506) in solution I but with 50 μM $CaCl_2$ added for 10 min. Smooth muscle cells were isolated by pipetting aortic pieces with a blunt-ended Pasteur pipette and placed in the middle of a glass coverslip coated with a solution containing laminin (20 μg/ml, L2020). Cells were loaded with fura-2-acetoxymethyl ester and analyzed as described previously (7).

Design of a small interference RNA and production of recombinant adeno-associated viruses. The multiple cloning site (MCS) of the vector N1-EGFP (BD Bioscience, Heidelberg, Germany) was removed by digestion with the restriction

enzymes NheI and AgeI. Cohesive ends were filled up by Klenow fragment and religated for the production of the N1-EGFPΔMCS vector. A cassette with a filled-up NotI site and a BspLU11 site containing the H1 promoter from the pSUPER vector (5) was then cloned into the linearized N1-EGFPΔMCS vector. After digestion with Acc65I and AflII cohesive ends were again filled up by Klenow fragment and cloned into the blunt ends of an HpaI and a filled-up XbaI site of the pHpa7 vector to generate the pH 1-EGFP-dsAAV2 vector.

Sequences for the production of an siRNA homologous to TRPC3 (indicated by underlining) were designed using the extended rule set of Reynolds et al. (25): siRNA TRPC3 sense (5′-GAT CCC CGT GTC AAA CTT GCC ATT AAT TCA AGA GAT TAA TGG CAA GTT TGA CAC TTT TTG GAA A) and siRNA TRPC3 antisense oligonucleotide (5′-AGC TTT TCC AAA AAG TGT CAA ACT TGC CAT TAA TCT CTT GAA TTA ATG GCA AGT TTG ACA CGG G).

Oligonucleotides were commercially synthesized, annealed, phosphorylated by T4 polynucleotide kinase, and inserted into the HindIII and BglII sites of the pH 1-EGFP-dsAAV2 vector.

Virus was generated using triple transfection of the p80XX6, the pAAV2/1, and the pH 1-EGFP-dsAAV2 vector into HEK 293 cells. Adeno-associated type 1 viruses were purified using a CsCl gradient. The virus titer was quantified by quantitative PCR, and 5×10^8 viruses were used to infect 3×10^5 cells.

Transfection of smooth muscle cells by electroporation. Smooth muscle cells from thoracic aortas of wild-type and TRPC6$^{-/-}$ mice were prepared as described above and nucleofected with pcDNA3 vectors coding for TRPC3GFP or TRPC6GFP. Control cells were electroporated with the pCDNA3-green fluorescent protein (GFP) vector. Electroporation was carried out by using a nucleofector (Amaxa GmbH, Cologne, Germany) and the protocol and solutions for human aortic smooth muscle cells (human AOSMC Nucleofector kit) as described by the supplier (Amaxa GmbH, Cologne, Germany).

Patch clamp recordings and preparation of cerebrovascular smooth muscle cells. Single smooth muscle cells were enzymatically isolated from cerebellar and basilar arteries of mice as described in detail elsewhere (24). Electrophysiological recordings were made essentially as described previously (7) using patch pipettes with resistances of 5.5 to 8.0 MΩ when filled with the intracellular solution (CsCl, 120 mM; NaCl, 9.4 mM; $MgCl_2$, 1 mM; Na_3GTP, 0.2 mM, buffered at 100 nM free Ca^{2+} with 10 mM BAPTA {*N*,*N*′-[1,2-ethanediylbis-(oxy-2,1-phenylene)]bis[*N*-(carboxymethyl)glycine]} and 10 mM HEPES, titrated to pH 7.2 by CsOH and with or without 1-stearoyl-2-arachidonoyl-*sn*-glycerol [SAG, 50 μM; Calbiochem, Darmstadt, Germany]). Patch clamp recordings were carried out on the stage of an inverted microscope (Olympus IX 70) at room temperature (23°C). Adherent smooth muscle cells were superfused in a cell culture dish mounted to a small perfusion chamber with the extracellular solution (NaCl, 140 mM; CsCl, 5 mM; $CaCl_2$, 2 mM; $MgCl_2$, 1 mM; glucose, 10 mM; HEPES, 10 mM; titrated to pH 7.4 with NaOH). Data from conventional whole-cell recordings were collected with an EPC10 patch clamp amplifier (HEKA, Lambrecht, Germany) using the Pulse software (HEKA). Patch pipettes made of borosilicate glass (Science Products, Hofheim, Germany) had resistances of 5.5 to 8.0 MΩ when filled with the intracellular solution (CsCl, 120 mM; NaCl, 9.4 mM; $MgCl_2$, 1 mM; Na_3GTP, 0.2 mM; buffered at 100 nM free Ca^{2+} with 10 mM BAPTA and 10 mM HEPES, titrated to pH 7.2 with CsOH) or the second intracellular solution containing additionally the potent non-membrane-permeable diacylglycerol derivate SAG. This intracellular solution with 50 μM SAG (Calbiochem, Darmstadt, Germany) had a dimethyl sulfoxide concentration of 0.05% and was sonicated for more than 7 min directly before pipette filling. The liquid junction potential was +4.3 mV, and the correction of this offset was made by the Pulse software. The cells were held at a potential of −60 mV, and current-voltage relations were obtained from triangular voltage ramps from −100 to +60 mV with a slope of 0.4 V s^{-1} applied at a frequency of 1 Hz. Data were acquired at a frequency of 5 kHz after filtering at 1.67 kHz.

For the Na^+-free extracellular solution, Na^+ was replaced by an equimolar concentration of *N*-methyl-D-glucamine ($NMDG^+$). Nimodipine (10 μM) was added to the standard extracellular solution to check for voltage-dependent Ca^{2+} currents activated by depolarizing ramps. Each of the Cl^- channel blockers 5-nitro-2-(3-phenyl-propylamino)-benzoate (NPPB), niflumic acid, and 4,4′-diisothiocyanostilbene-2,2′-disulfonic acid (DIDS) was tested in the standard extracellular solution to analyze the contribution of Cl^- currents to whole-cell currents by applying ramps.

Membrane potentials from isolated cerebral smooth muscle cells were recorded using the conventional whole-cell configuration at an acquisition rate of 200 Hz for more than 10 min. To imitate physiological conditions, current clamp measurements were performed with the intracellular solution (KCl, 80 mM; potassium glutamate, 50 mM; $MgCl_2$, 2 mM; MgATP, 2 mM; HEPES, 10 mM; buffered at 100 nM free Ca^{2+} with 10 mM BAPTA, titrated to pH 7.2 by KOH) and the extracellular solution (NaCl, 140 mM; KCl, 5.4 mM; $MgCl_2$, 1 mM; $CaCl_2$, 2 mM; glucose, 10 mM; and HEPES, 10 mM; titrated to pH 7.4 with NaOH). The liquid junction potential was +8.0 mV. Criteria for the acceptance of recordings were (i) stable membrane potentials for at least 5 min, (ii) membrane potentials of ≤−20 mV, and (iii) membrane potentials with one bell-shaped frequency distribution.

Inositol 1,4,5-trisphosphate (IP3)-induced store-operated membrane currents in freshly isolated smooth muscle cells of brain arteries were also analyzed by the whole-cell patch clamp technique. Pipette infusions were made by adding 100 μM IP3 into the SAG-free pipette solution. To exclude calcium-induced effects on membrane currents, the free calcium was buffered to 100 nM by BAPTA. For some recordings we used an IP3-containing SAG-free pipette solution with less chloride which was replaced equimolarly with methanosulfate. The fold amplification of current densities at ±60 mV was calculated as the quotient of the mean of current densities from 0 to 5 and from 120 to 125 s after patch rupture.

The osmolarity of all solutions was measured with the vapor osmometer Vapro 5520 (Wescor Inc.) to be in the range of 294 to 309 mosmol l^{-1}.

Statistical analysis. Error bars represent standard errors of the means (SEM). Statistical analysis was performed using an unpaired Student *t* test, and significance was accepted at $P < 0.05$ (two-tailed *P* value), if not stated otherwise.

RESULTS

Targeted disruption of the mTRPC6 gene. The *TRPC6* gene was inactivated by gene targeting in murine ES cells. Replacement of exon 7 with a positive selection marker (PGK-Neo) resulted in loss of the region coding for amino acids 584 to 670 that form transmembrane segments 4 and 5 and a small part of the pore domain (Fig. 1A). A heterozygous ES clone (48F) was identified by Southern blotting (Fig. 1B). This clone was devoid of vector (pBS) or PGK-Neo DNA elsewhere in the genome (Fig. 1B) and showed integration of the PGK-Neo sequence at the correct site as shown by screening with both the 5′ external probes and the Neo probe (Fig. 1B). Heterozygous and homozygous knockout mice were identified by PCR analysis of DNA extracted from tail biopsy samples using appropriate primer pairs (Fig. 1C, left and right panels). Using primer pairs F/R 1 to 3, we were not able to amplify parts of the TRPC6 mRNA upstream and downstream of the deleted exon 7 by RT-PCR analysis of total RNA from lungs of *TRPC6*$^{-/-}$ mice. Expected PCR products, indicative of intact TRPC6 mRNA, were obtained from RNA of WT mice (Fig. 1D).

Taking advantage of a procedure analyzing TRPC channels in rat brain microsomal proteins (27), we detected a band migrating with a molecular mass of approximately 110 kDa, the expected size of TRPC6, in TRPC6WT but not in embryonic brains of *TRPC6*$^{-/-}$ mice (Fig. 1E).

TRPC6$^{-/-}$ mice are viable and show no gross phenotype. Fertility and litter sizes were normal compared to those of TRPC6WT mice.

Contractility of aortic and mesenteric rings. Subsequently, we explored the behavior of vascular smooth muscle, as seen in aortic rings stimulated with increasing concentrations of the α_1-adrenoceptor agonist phenylephrine. Agonist-induced contractility was increased ($P < 0.05$ at 0.3 to 100 μM phenylephrine) in aortic rings from TRPC6-deficient mice compared to wild-type controls (Fig. 2A). While overall contraction in response to 3 μM phenylephrine was reduced in the presence of 100 μM $CdCl_2$, a blocker of voltage-gated Ca^{2+} channels, the increased responsiveness of aortic rings from TRPC6-deficient mice was still observed (Fig. 2B, $P < 0.05$). To examine small peripheral resistance blood vessels, we isolated mesenteric arteries and monitored phenylephrine-dependent smooth muscle

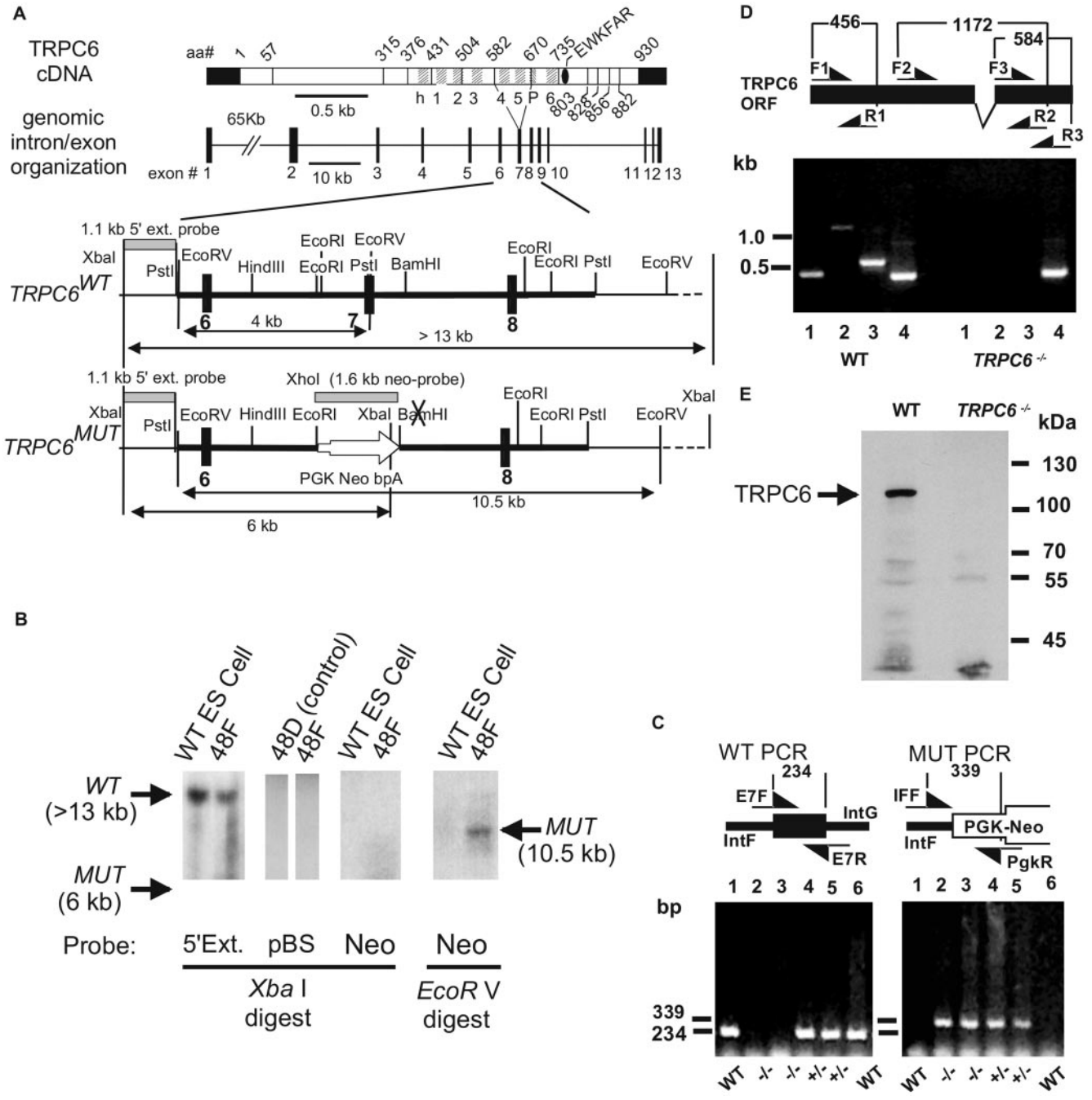

FIG. 1. Targeted disruption of the murine *TRPC6* gene. (A) cDNA with delineation of intron-exon boundaries and location of hydrophobic segments presumed to code for transmembrane domains, genomic organization of the *TRPC6* gene, and restriction maps of the *mTRPC6* target locus before (WT) and after (MUT) targeting. Exons and introns are shown as filled boxes and lines, respectively. Exon 7 of the *mTRPC6* gene contains the coding region of the depicted amino acid sequence of the mTRPC6 protein. The targeting vector contains 8.7 kb of murine *TRPC6* genomic sequence (bold line in all restriction maps). The 5′ external and the Neo probe used for the Southern analysis are indicated by gray bars. (B) Identification of targeted ES cell clone 48F by Southern blot analysis. As controls, WT ES cells and clone 48D with a misintegrated targeting vector are shown. (C) Agarose gel electrophoresis of PCR products identifying the genotypes of the F_2 generation from a chimera obtained from the targeted 48F ES cell clone. Approximate locations of the genotyping primers are shown in the diagram above the photograph of the electrophoretic separation of the PCR products. (D) Analysis of RT-PCR products by agarose gel electrophoresis identifying the indicated regions of the TRPC6 mRNA in total RNA from lung cells of WT and TRPC6-deficient (*TRPC6*$^{-/-}$) mice. The coding region of exon 7 is deleted in the diagram showing the approximate locations of primers. Lanes 1 to 3 show PCR products using primer pairs F1/R1, F2/R2, and F3/R3, respectively; lane 4 shows RT-PCR products obtained by using primers for β-actin. (E) Immunoblot analysis of equal amounts of brain microsomal proteins from wild-type and *TRPC6*$^{-/-}$ embryos by a TRPC6-specific antiserum.

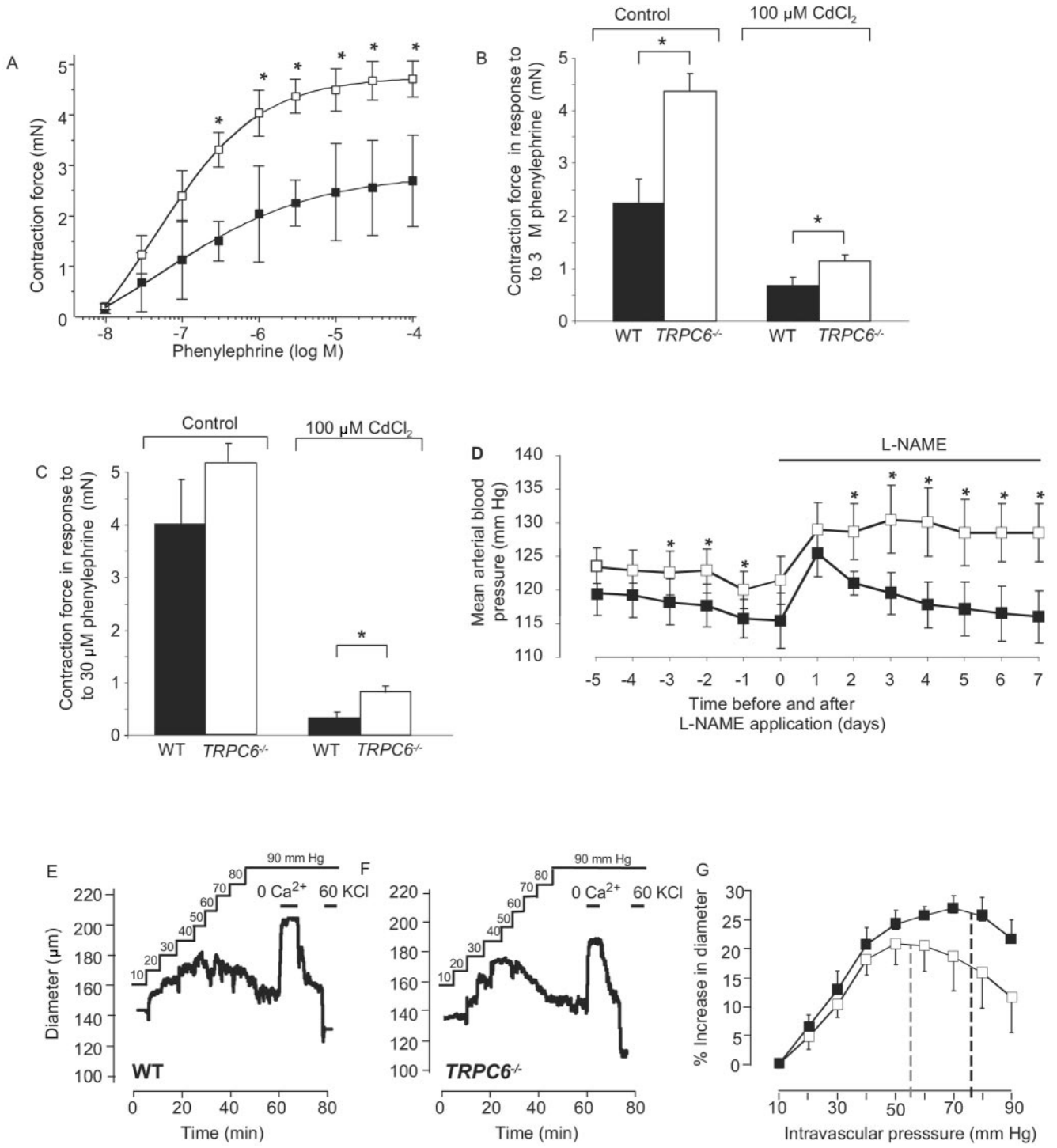

FIG. 2. Vascular smooth muscle properties in wild-type and *TRPC6*$^{-/-}$ mice. Agonist-induced vasoconstriction of aortic rings (A and B) and mesenteric arteries (C), telemetric measurement of mean blood pressure (D), and vasoconstriction in response to intravascular pressure (E, F, and G). (A) Response of aortic rings from wild-type (black squares, $n = 14$) and *TRPC6*$^{-/-}$ mice (white squares, $n = 21$) to increasing concentrations of phenylephrine; values are in mN ± SEM. (B) Summary of the contractility of aortic rings from wild-type (WT) and *TRPC6*$^{-/-}$ mice after application of phenylephrine in the absence (WT [black bar], $n = 13$; *TRPC6*$^{-/-}$ [white bar], $n = 21$) and in the presence of $CdCl_2$ (WT [black bar], $n = 7$; *TRPC6*$^{-/-}$ [white bar], $n = 12$). Significant differences at $P < 0.05$ are indicated by asterisks. (C) Summary of contractility of mesenteric arteries from wild-type and *TRPC6*$^{-/-}$ mice after application of phenylephrine in the absence (WT, black bar, eight arteries from four mice; *TRPC6*$^{-/-}$, white bar, 12 arteries from six mice) and in the presence of $CdCl_2$ (WT, black bar, eight arteries from four mice; *TRPC6*$^{-/-}$, white bar, 10 arteries from five mice) before and during contraction. Significant differences are indicated by asterisks (* for $P < 0.05$). (D) Telemetric analysis of the mean arterial blood pressure in control (WT or *TRPC6*$^{+/-}$) and *TRPC6*$^{-/-}$ mice. Blood pressure of control ($n = 5$, black squares) and *TRPC6*$^{-/-}$ ($n = 7$, white squares) mice was continuously recorded under basal conditions and after applying L-NAME to the drinking water (control, $n = 4$; *TRPC6*$^{-/-}$, $n = 6$). Further details are indicated in Materials and Methods. Significant differences are indicated by asterisks

contractility. In the presence of $CdCl_2$, the phenylephrine (30 μM)-induced contractile force of arteries from *TRPC6*$^{-/-}$ mice was significantly higher than that of wild-type littermates (Fig. 2C, $P < 0.05$).

Mean arterial blood pressure. Following a recovery period of 5 days after implantation of telemetric sensors, TRPC6-deficient mice were found to have a significantly higher mean arterial blood pressure on days 3, 2, and 1 before L-NAME treatment ($P < 0.05$, evaluated by analysis of variance and Duncan's multiple range test) (Fig. 2D) with basal values of 116 ± 1 mm Hg and 123 ± 1 mm Hg for the control and *TRPC6*$^{-/-}$ mice, respectively. Administration of the nitric oxide synthase inhibitor L-NAME caused an increase in blood pressure in *TRPC6*$^{-/-}$ and wild-type mice, with significantly higher values on days 2, 3, 4, 5, 6, and 7 ($P < 0.05$, evaluated by analysis of variance and Duncan's multiple range test) in *TRPC6*$^{-/-}$ mice, resulting in an average value of 116 ± 4 mm Hg and 129 ± 4 mm Hg on day 7 for control and *TRPC6*$^{-/-}$ mice, respectively.

Myogenic tone of cerebral arteries. We directly monitored the effect of intravascular pressure on the diameter of cerebral arteries from wild-type and TRPC6-deficient mice and found that intravascular pressure induced a similar degree of vasoconstriction in *TRPC6*$^{-/-}$ and control mice (Fig. 2E and F). The pressure at which myogenic dilatation reversed into myogenic constriction due to the Bayliss effect was significantly ($P < 0.05$) shifted to the left towards lower values in *TRPC6*$^{-/-}$ vessels compared to wild-type cerebral arteries (55 ± 6 mm Hg versus 78 ± 5 mm Hg, Fig. 2G). The constriction of brain arteries was relieved in the absence of external Ca^{2+}, and blood vessels were fully constricted in response to depolarization by 60 mM KCl (Fig. 2E and F).

Quantitative assessment of TRPC mRNAs in TRPC6-deficient mice. To gain insight into molecular mechanisms resulting in the phenotype of *TRPC6*$^{-/-}$ mice described above, we next quantified mRNA levels of all seven TRPCs in thoracic aortas and cerebral arteries of *TRPC6*$^{-/-}$ and wild-type mice (Fig. 3). Subsequently, transcription of *TRPC* genes was compared by means of real-time quantitative PCR. TRPC1, -3, and -6 constituted the predominant complement of TRPC channels in thoracic aortas (Fig. 3A). Most *TRPC* genes as well as the $Ca_V1.2\alpha_1$ subunit genes were transcribed at similar levels in wild-type and TRPC6-deficient mice. However, the TRPC3 mRNA level was elevated three- to fivefold in *TRPC6*$^{-/-}$ mice ($P < 0.05$; Fig. 3A) concomitant with an additional twofold up-regulation of aortic TRPC7 mRNA ($P < 0.05$) (Fig. 3A). Along these lines a twofold up-regulation ($P < 0.05$) of TRPC3 was also detectable in cerebral arteries (Fig. 3B). In contrast to these results, mRNA expression of TRPM4, another TRP channel involved in myogenic constriction of cerebral arteries (8), was not elevated in *TRPC6*$^{-/-}$ mice compared to wild-type mice (data not shown). Thus, increased contractility of vascular smooth muscle in TRPC6-deficient mice is correlated with an up-regulation of TRPC3/7-type mRNAs in aortas and cerebral arteries.

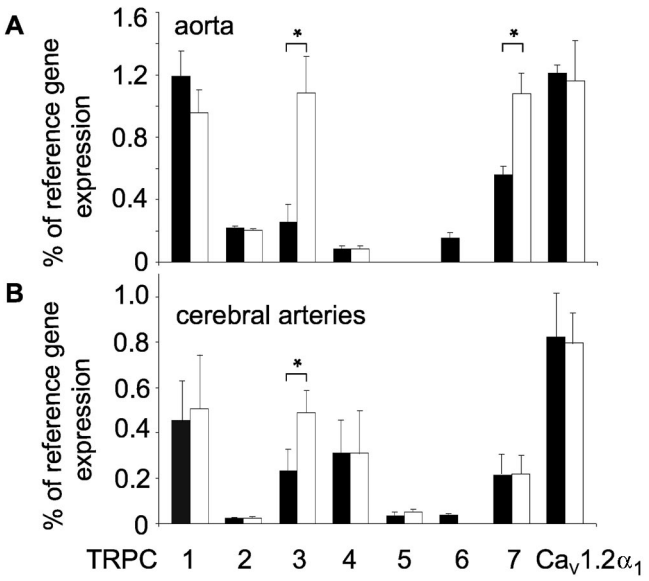

FIG. 3. Quantitative analysis of mRNA levels by real-time PCR of total RNA from thoracic aortas (A) and cerebral arteries (B). Total RNA was prepared from WT (thoracic aortas, $n = 4$; cerebral arteries, $n = 4$, black bars) and *TRPC6*$^{-/-}$ (thoracic aortas, $n = 5$; cerebral arteries, $n = 5$, white bars) mice and reverse transcribed, and products of the first-strand synthesis were analyzed for the presence of amplification products obtained with primer pairs described under Materials and Methods. mRNAs coding for TRPCs, β-actin (as reference gene), and the $Ca_V1.2\alpha_1$ subunit were quantified with the aid of a light cycler. Values are presented as percentage of reference mRNA expression (β-actin mRNA expression). Error bars indicate SEM. Significant differences are indicated by asterisks (* for $P < 0.05$).

Functional analysis of TRPC3-type channels at the cellular level. Smooth muscle cells from thoracic aortas were isolated, and Ba^{2+} influx was monitored in the presence of 100 μM $CdCl_2$ in fura-2-loaded single smooth muscle cells. Basal influx of Ba^{2+} ions was profoundly increased in smooth muscle cells isolated from TRPC6-deficient compared to wild-type mice (Fig. 4A). Similar results were obtained by analyzing Ba^{2+} influx into smooth muscle cells freshly isolated from cerebral arteries of TRPC6-deficient and wild-type mice (data not shown). The basal influx was further stimulated in both cell types by the addition of the membrane-permeable DAG analogue 1-oleoyl-2-acetyl-*sn*-glycerol (OAG, 100 μM) (inset of Fig. 4A). Cultured smooth muscle cells of *TRPC6*$^{-/-}$ mice infected with adeno-associated viruses either coding for GFP or carrying an siRNA expression cassette directed against the TRPC3 mRNA plus GFP were further analyzed. Expression of TRPC3-siRNA in these cells resulted in decreased basal activ-

(* for $P < 0.05$). (E to G) Myogenic tone of cerebral arteries after application of intravascular pressure (E and F). Representative traces of diameter recordings in cerebral arteries from a wild-type (E) and a *TRPC6*$^{-/-}$ (F) mouse. The solid black line represents the intravascular pressure applied. Where shown, extracellular Ca^{2+} was removed (nominal 0 Ca^{2+}) or 60 mM KCl (60 KCl) was added. (G) Summary of increases in diameters after application of intravascular pressure to cerebral arteries from wild-type (black squares, $n = 6$) and *TRPC6*$^{-/-}$ (white squares, $n = 6$) mice. The shift from vasodilatation to vasoconstriction due to the Bayliss effect is indicated by dashed lines for wild-type (black) and *TRPC6*$^{-/-}$ (gray) mice. The shift was determined by data point fitting using polynomic approximation.

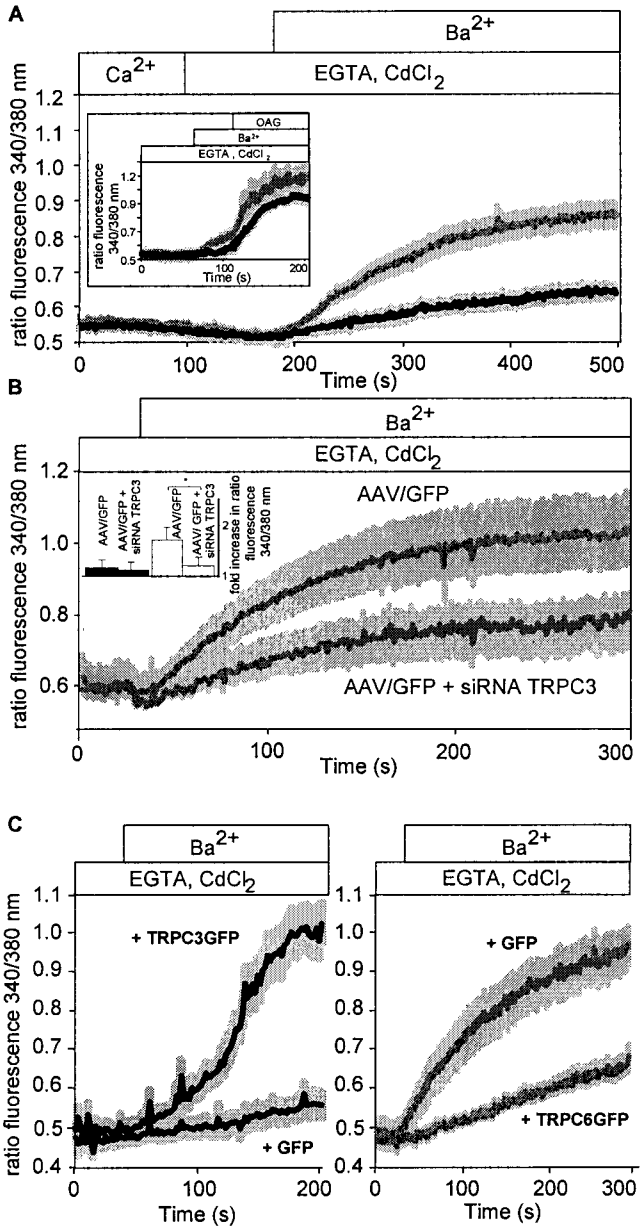

FIG. 4. Ba^{2+} influx into isolated smooth muscle cells from control and *TRPC6*$^{-/-}$ mice. (A) Ba^{2+} influx into isolated smooth muscle cells from thoracic aortas of control and *TRPC6*$^{-/-}$ mice. Isolated cells were loaded with fura-2, and basal Ba^{2+} influx was assessed by the increase in fluorescence ratios. After application of EGTA (2 mM) and $CdCl_2$ (100 μM) in a nominally Ca^{2+}-free solution, Ba^{2+} (2 mM) was added to the bath solution. The black (WT, $n = 12$ cells from three mice) and gray (*TRPC6*$^{-/-}$, $n = 14$ cells from four mice) lines represent the calculated means, whereas the light gray areas indicate SEM. (A, inset) Ba^{2+} influx into smooth muscle cells from thoracic aortas isolated from *TRPC6*$^{-/-}$ mice (gray trace, $n = 5$ cells from three mice) and wild-type mice (black trace, $n = 10$ cells from three mice) loaded with fura-2 and analyzed by single-cell fluorescence imaging. After application of EGTA and $CdCl_2$ in a nominally Ca^{2+}-free solution, Ba^{2+} was added to the bath solution and cells were stimulated with OAG (100 μM) as indicated. (B) Ba^{2+} influx into cultured smooth muscle cells from thoracic aortas of *TRPC6*$^{-/-}$ mice infected with adeno-associated viruses expressing the green fluorescent protein (AAV/GFP, gray trace, $n = 12$ cells from five mice) or a TRPC3-specific small interference RNA plus GFP (AAV/GFP + siRNA TRPC3, gray trace, $n = 12$ cells from five mice). (B, inset) Comparison of fold increases in basal activities in cultured smooth muscle cells from wild-type (black bars) and *TRPC6*$^{-/-}$ (white bars) aortas after infection with AAV/GFP or AAV/GFP + siRNA TRPC3. Data were obtained 1 s and 300 s after starting the experiment. (C) Ba^{2+} influx in cultured smooth muscle cells from thoracic aortas of wild-type mice (left panel) and *TRPC6*$^{-/-}$ mice (right panel) electroporated with a pCDNA3 vector coding for TRPC3GFP (+ TRPC3GFP) or GFP (+ GFP) (left panel) and TRPC6GFP (+ TRPC6GFP) or GFP (+ GFP) (right panel). Black (WT, $n = 10$ cells from five mice) and gray (*TRPC6*$^{-/-}$, $n = 11$ cells from five mice) lines represent the calculated means, whereas the light gray areas indicate SEM.

ity (Fig. 4B) compared to *TRPC6*$^{-/-}$ cells expressing GFP alone, although receptor-operated ion influx remained unchanged (data not shown). While TRPC3-siRNA expression had no significant effect on basal Ba^{2+} influx in wild-type cells, TRPC3-siRNA expression significantly decreased basal activity in *TRPC6*$^{-/-}$ cells (Fig. 4B, inset). Specific down-regulation of TRPC3 but not TRPC7 protein expression by siRNA molecules directed against TRPC3 was demonstrated in HEK 293 cells heterologously expressing TRPC3 or TRPC7 (data not shown). These results indicate that TRPC3 expression alone is responsible for the high basal activity of *TRPC6*$^{-/-}$ smooth muscle cells from thoracic aortas. As expected, expression of TRPC3 in wild-type cells resulted in increased basal activity (Fig. 4C, left panel), while TRPC6 expression in *TRPC6*$^{-/-}$ smooth muscle cells reduced basal cation influx (Fig. 4C, right panel).

We next monitored whole-cell currents in freshly isolated cerebral artery smooth muscle cells. Ion currents with a curvilinear current-voltage relationship reversing around 0 mV, reminiscent of TRPC3 and -6, were recorded in cells from both *TRPC6*$^{-/-}$ and wild-type mice (Fig. 5A, left panel). The capacitance of the cell membrane did not differ between smooth muscle cells derived from either source (6.6 ± 0.3 pF for both wild-type and *TRPC6*$^{-/-}$ cells). However, an increase in basal current density was discernible at −60 mV ($P = 0.04$) and at +60 mV ($P = 0.02$) when *TRPC6*$^{-/-}$ mice were compared to control mice (Fig. 5B, left). To activate DAG-sensitive TRPC channels in smooth muscle cells, we included the endogenous, membrane-impermeable, and potent DAG analogue SAG (50 μM) in the pipette solution, resulting in enhanced inward and outward currents (Fig. 5A, right panel). Current densities of SAG-stimulated cerebral smooth muscle cells were larger at −60 mV ($P < 0.05$) as well as at +60 mV ($P < 0.001$) in *TRPC6*$^{-/-}$ mice than in their wild-type and *TRPC6*$^{+/-}$ littermates (Fig. 5B, right).

Current densities were potentiated in a divalent (nominally Ca^{2+}- and Mg^{2+}-free medium) free medium consistent with the expression of TRPC3 and TRPC6, which are both inhibited by extracellular Ca^{2+} (data not shown). Basal and DAG-dependent inward currents were fully NMDG sensitive. They were not mediated by L-type voltage-gated Ca^{2+} channels, because 10 μM nimodipine, a blocker of voltage-dependent Ca^{2+} channels, did not affect currents recorded during voltage ramps in control and *TRPC6*$^{-/-}$ cells in the absence or presence of SAG ($n = 18$, $n \geq 4$ for each combination). Likewise, none of three Cl^- channel blockers, NPPB (50 μM, $n = 19$), niflumic acid (100 μM, $n = 16$), and DIDS (300 μM, $n = 13$), had an effect on inward and outward currents ($n \geq 3$ for

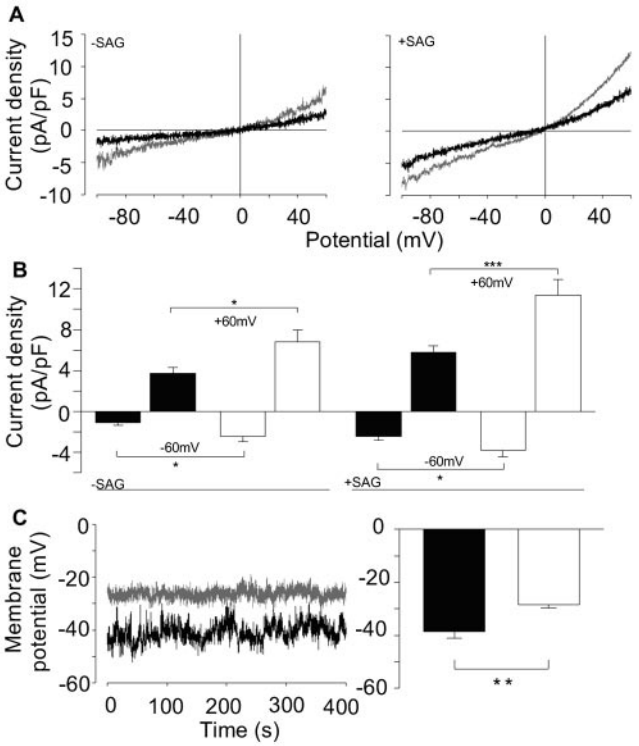

FIG. 5. (A and B) Analysis of current densities by electrophysiological analysis of single smooth muscle cells isolated from cerebral arteries of control (black traces) or *TRPC6*$^{-/-}$ (gray traces) mice in the absence (A, left panel) or presence (50 μM) (A, right panel) of SAG. (B) Summary of current densities of single smooth muscle cells isolated from control (black bars, $n = 12$ cells from eight animals) or *TRPC6*$^{-/-}$ (white bars, $n = 12$ cells from four animals) mice in the absence (−SAG, left) or in the presence (+SAG, right) of SAG (control, $n = 25$ cells from six animals; *TRPC6*$^{-/-}$, $n = 19$ from four animals). Significant differences are indicated by asterisks (* for $P < 0.05$ and *** for $P < 0.001$). (C, left) Representative traces of recorded membrane potentials in single wild-type (black trace) and *TRPC6*$^{-/-}$ (gray trace) cerebral smooth muscle cells. (C, right) Summary of membrane potentials in isolated smooth muscle cells from control (black bar, $n = 20$ cells from five animals) and *TRPC6*$^{-/-}$ (white bar, $n = 12$ cells from four animals) mice. Significant differences are indicated by asterisks (** for $P < 0.01$).

control and *TRPC6*$^{-/-}$ cells in the absence or presence of SAG). Finally, addition of 5 μM $GdCl_3$ to the bath solution inhibited inward currents at −60 mV by no more than 5 to 12% ($n \geq 10$), excluding a significant contribution of store-operated Ca^{2+}-permeable channels to the currents measured (data not shown).

By infusion of IP3 endogenous currents were increased. The relative increases in current densities after 120 s were not significantly different ($P = 0.70$ at +60 mV and $P = 0.70$ at −60 mV), being 3.9 ± 0.8 at 60 mV and 3.8 ± 1.1 at −60 mV in cells from *TRPC6*$^{+/-}$ and 3.6 ± 0.3 at 60 mV and 3.2 ± 0.7 at −60 mV in cells from *TRPC6*$^{-/-}$ mice (data not shown). Thus, it is very unlikely that TRPC6 is involved in store-operated currents activated by IP3 in these cells.

To examine the functional consequences of the described basal activity in a physiological setting, we monitored the membrane potential in isolated smooth muscle cells from cerebral arteries (Fig. 5C, left panel). The mean membrane potentials in smooth muscle cells from *TRPC6*$^{-/-}$ mice were significantly ($P < 0.01$) more depolarized (−28.3 ± 1.4 mV [$n = 12$]) than those in smooth muscle cells of wild-type littermates (−38.6 ± 2.4 mV [$n = 20$]; Fig. 5C, right panel). The depolarized potential of *TRPC6*$^{-/-}$ smooth muscle cells most probably results from a higher TRPC3-mediated cation influx.

DISCUSSION

We provide the first mouse model deficient in the receptor-activated nonselective cation channel TRPC6. Because TRPC6 is highly expressed in smooth muscle cells and has been suggested to represent an integral part of receptor-operated cation channels in vascular smooth muscle (12, 16, 18, 29), we embarked on a detailed analysis of vascular smooth muscle function in *TRPC6*$^{-/-}$ mice. Surprisingly, we detected an enhanced responsiveness of smooth muscle to constrictor agonists on the thoracic aorta of *TRPC6*$^{-/-}$ mice. Physiologically, the increased tone and sensitivity of smooth muscle to constrictor agonists resulted in a higher elevated mean arterial blood pressure and a shift of the onset of the myogenic tone in cerebral arteries towards lower intravascular pressures. These physiological responses were associated with an up-regulation of TRPC3-type channels in vascular smooth muscle in *TRPC6*$^{-/-}$ mice.

Despite their high degree of structural and functional similarity, TRPC3, -6, and -7 differ substantially in their basal channel activities. While TRPC6 is a tightly regulated receptor-activated cation channel (7), TRPC3 and TRPC7 display considerable constitutive activity upon expression in various cell lines (7, 23, 33; summarized in reference 28), and we have recently shown that a discrepant N-linked glycosylation pattern is a major determinant for basal TRPC3 and TRPC6 activities (7).

To determine whether ablation of TRPC6 expression and replacement by TRPC3 and TRPC7 would increase TRPC-dependent cation fluxes in smooth muscle cells of *TRPC6*$^{-/-}$ mice, we monitored basal and OAG-stimulated Ba^{2+} influx and the electrophysiological properties of single TRPC6-deficient smooth muscle cells. We show that basal Ba^{2+} influx was substantially elevated compared to control cells. The expression of a TRPC3-specific siRNA in *TRPC6*$^{-/-}$ cells resulted in a reduced basal activity indistinguishable from that of wild-type cells, indicating that TRPC3 channel activity alone might be responsible for the discrepant behavior of TRPC6-deficient smooth muscle cells. Along these lines, expression of TRPC3 in wild-type cells resulted in increased basal activity, whereas TRPC6 expression in *TRPC6*$^{-/-}$ smooth muscle cells reduced basal cation influx. These data favor the concept of the formation of TRPC3/6 heteromeric complexes with a tightly receptor-operated TRPC6 subunit suppressing TRPC3 basal activity (7). The ineffectiveness of a TRPC6 siRNA in increasing basal influx in wild-type smooth muscle cells strongly argues for a long-term adaptation process to the loss of TRPC6, resulting in TRPC3 up-regulation (data not shown). Ba^{2+} influx was increased further by application of a membrane-permeable DAG analogue. The OAG response demonstrated that TRPC3-type channels expressed in TRPC6-deficient cells are functional. In accord with these observations, whole-cell patch clamp recordings on cerebral artery smooth muscle cells re-

vealed higher TRPC-mediated current densities in *TRPC6*$^{-/-}$ mice than in control mice. The augmented cation influx results in a more depolarized membrane potential, probably leading to a higher open probability of voltage-gated L-type Ca^{2+} channels in vascular smooth muscle cells, thus explaining the higher smooth muscle contractility and the increased sensitivity of cerebral arteries to intravascular pressure. All our data support the hypothesis that, in the TRPC6-deficient mice, constitutively active TRPC3-type channels are not able to functionally replace TRPC6, resulting in a higher basal cation influx, increased sensitivity towards constrictor agonists, and enhanced contractility of vascular smooth muscle.

Although we can only speculate about the molecular composition of a native TRPC6-containing channel complex in smooth muscle cells, expression studies show coexpression with TRPC3 in most of the analyzed smooth muscle tissues and derived cell lines (summarized in reference 2). Most interestingly, recent multimerization data show that TRPC3/6 tetramers are formed in a heterologous expression system (14), in brain synaptosomes (9), and in polarized epithelial cells (1). Our findings are fully compatible with the hypothesis that, in such heteromultimeric complexes, TRPC6 may suppress the high basal activity of TRPC3, leading to a tightly receptor-regulated cation channel complex required for the physiological regulation of smooth muscle tone. It is notable that, in the *Drosophila melanogaster* eye, a similar mechanism has been proposed to generate the phospholipase C-regulated cation conductance via a TRPL/TRPγ complex, because either channel protein is constitutively active when expressed alone (30).

Activation of nonselective cation channels in vascular smooth muscle cells subsequent to receptor activation or rises of intravascular pressure leads to depolarization and consecutive recruitment of voltage-gated L-type Ca^{2+} channels mediating Ca^{2+} influx and smooth muscle contraction (summarized in reference 12). Voltage-gated Ca^{2+} channels are key components of the vasopressor response sequence as illustrated by the effectiveness of Ca^{2+} channel blockers and K^+ channel openers in the treatment of hypertension. Nevertheless, smooth muscle tone is critically determined by TRPC3 and TRPC6 channels. In line with this concept TRPC6 and TRPC3 were found to be up-regulated in lung tissues and vascular smooth muscle cells of patients suffering from idiopathic pulmonary arterial hypertension (31).

In the present study, we provide comprehensive evidence that TRPC3 and TRPC6 are functionally nonredundant and that TRPC6 plays a unique role in the physiological control of vascular smooth muscle tone. Thus, TRPC3 and TRPC6 may represent interesting new drug targets to reduce smooth muscle tone in pathophysiological conditions such as hypertension (26, 31).

ACKNOWLEDGMENTS

We thank Sumit Sen for the initial characterization of P1 clones and Guylain Boulay, Meisheng Jiang, and Karsten Spicher for their technical advice during the production and breeding of TRPC6-deficient mice. We also thank Tim Plant for helpful discussion and critical advice on the manuscript. The help of Heribert Nau, Kim Ngo, and Rafi Salibian in the genotyping of mice is greatly acknowledged. We are grateful to Christan Walther for his initial help in preparing smooth muscle cells from cerebral arteries and Serdar Sel and Berit Schuhmann for their support in performing light cycler experiments. The excellent technical assistance of Sabine Grüger, Diana Herold, Ilona Kamer, and Winfried Lorenz is greatly appreciated.

This work was supported by the Deutsche Forschungsgemeinschaft (A.D., T.G., and M.G.) and by a grant from the National Heart, Lung and Blood Institute, U.S. Department of Health and Human Services, to L.B. (HL-45198).

ADDENDUM IN PROOF

While *TRPC6*$^{-/-}$ mice lack full-length mRNA, it is possible to detect traces of TRPC6 mRNA 5′ to the neomycin cassette in some tissues of *TRPC6*$^{-/-}$ mice using primers F4 (nt positions 137 to 156) and R4 (nt positions 1422 to 1441). However, neither full-length TRPC6 nor accumulation of truncated 50-60 kDa proteins as predicted by the shortened mRNA is detectable in *TRPC6*$^{-/-}$ mice with antibodies directed against an N-terminal epitope as shown for brain (Fig. 1E). mRNA derived from sequences downstream of the neomycin cassette encoding the ion channel pore-forming region cannot be amplified in *TRPC6*$^{-/-}$ mice.

REFERENCES

1. **Bandyopadhyay, B. C., W. D. Swaim, X. Liu, R. Redman, R. L. Patterson, and I. S. Ambudkar.** 2005. Apical localization of a functional TRPC3/TRPC6-Ca^{2+}-signaling complex in polarized epithelial cells: role in apical Ca^{2+} influx. J. Biol. Chem. **280:**12908–12916.
2. **Beech, D. J., M. Muraki, and R. Flemming.** 2004. Non-selective cationic channels of smooth muscle and the mammalian homologues of *Drosophila* TRP. J. Physiol. **599:**685–706.
3. **Boulay, G., D. M. Brown, N. Qin, M. Jiang, A. Dietrich, M. X. Zhu, Z. Chen, M. Birnbaumer, K. Mikoshiba, and L. Birnbaumer.** 1999. Modulation of Ca^{2+} entry by polypeptides of the inositol 1,4,5-trisphosphate receptor (IP_3R) that bind transient receptor potential (TRP): evidence for roles of TRP and IP_3R in store depletion-activated Ca^{2+} entry. Proc. Natl. Acad. Sci. USA **96:**14955–14960.
4. **Boulay, G., X. Zhu, M. Peyton, M. Jiang, R. Hurst, E. Stefani, and L. Birnbaumer.** 1997. Cloning and expression of a novel mammalian homolog of Drosophila transient receptor potential (Trp) involved in Ca^{2+} entry secondary to activation of receptors coupled by the G_q class of G protein. J. Biol. Chem. **272:**29672–29680.
5. **Brummelkamp, T. R., R. Bernards, and R. Agami.** 2002. A system for stable expression of short interfering RNAs in mammalian cells. Science **296:**550–553.
6. **Clapham, D.** 2003. TRP channels as cellular sensors. Nature **426:**517–524.
7. **Dietrich, A., M. Mederos y Schnitzler, J. Emmel, H. Kalwa, T. Hofmann, and T. Gudermann.** 2003. N-linked protein glycosylation is a major determinant for basal TRPC3 and TRPC6 channel activity. J. Biol. Chem. **278:**47842–47852.
8. **Earley, S., B. J. Waldron, and J. E. Brayden.** 2004. Critical role of transient receptor potential channel TRPM4 in myogenic constriction of cerebral arteries. Circ. Res. **95:**922–929.
9. **Goel, M., W. G. Sinkins, and W. P. Schilling.** 2002. Selective association of TRPC channel subunits in rat brain synaptosomes. J. Biol. Chem. **277:**48303–48310.
10. **Gollasch, M., G. C. Wellmann, H. C. Knot, J. H. Jaggar, D. H. Damon, A. D. Bonec, and M. T. Nelson.** 1998. Ontogeny of local sarcoplasmic reticulum Ca^{2+} signals in cerebral arteries: Ca^{2+} sparks as elementary physiological events. Circ. Res. **83:**104–114.
11. **Gross, V., R. Plehm, J. Tank, J. Jordan, A. Diedrich, M. Obst, and F. C. Luft.** 2002. Heart rate variability and baroreflex function in AT_2 receptor-disrupted mice. Hypertension **40:**207–213.
12. **Gudermann, T., M. Mederos y Schnitzler, and A. Dietrich.** 2004. Receptor-operated cation entry—more than esoteric terminology? Science STKE *243:* pe35.
13. **Hoenderop, J. G., T. Voets, S. Hoefs, F. Weidema, J. Prenen, B. Nilius, and R. J. M. Bindels.** 2003. Homo- and heterotetrameric architecture of the epithelial Ca^{2+} channels TRPV5 and TRPV6. EMBO J. **22:**776–785.
14. **Hofmann, T., M. Schaefer, G. Schultz, and T. Gudermann.** 2002. Subunit composition of mammalian transient receptor potential channels in living cells. Proc. Natl. Acad. Sci. USA **99:**7461–7466.
15. **Hofmann, T., A. G. Obukhov, M. Schaefer, C. Harteneck, T. Gudermann, and G. Schultz.** 1999. Direct activation of human TRPC6 and TRPC3 channels by diacylglycerol. Nature **397:**259–263.
16. **Inoue, R., T. Okada, H. Onoue, Y. Hara, S. Shimizu, S. Naitoh, Y. Ito, and Y. Mori.** 2001. The transient receptor potential protein homologue TRP6 is the essential component of vascular α_1-adrenoceptor-activated Ca^{2+}-permeable cation channel. Circ. Res. **88:**325–332.

17. **Jiang, M., K. Spicher, G. Boulay, A. Martin-Requero, C. A. Dye, U. Rudolph, and L. Birnbaumer.** 2002. Mouse gene knockout and knockin strategies in application to α subunits of G_i/G_o family of G proteins. Methods Enzymol. **344:**277–298.
18. **Jung, S., R. Strotmann, G. Schultz, and T. D. Plant.** 2002. TRPC6 is a candidate channel involved in receptor-stimulated cation currents in A7r5 smooth muscle cells. Am. J. Physiol. Cell Physiol. **282:**C347–C359.
19. **Löhn, M., G. Dubrovska, B. Lauterbach, F. C. Luft, M. Gollasch, and A. M. Sharma.** 2002. Periadventitial fat releases a vascular relaxing factor. FASEB J. **16:**1057–1063.
20. **Löhn, M., D. Kampf, C. Gui-Xuan, H. Haller, F. C. Luft, and A. M. Gollasch.** 2002. Regulation of arterial tone by smooth muscle myosin type II. Am. J. Physiol. Cell Physiol. **283:**C1383–C1389.
21. **Loufrani, L., K. Matrougi, Z. Li, B. I. Levy, P. Lacolley, D. Paulin, and D. Henrion.** 2002. Selective microvascular dysfunction in mice lacking the gene encoding for desmin. FASEB J. **16:**117–119.
22. **Montell, C., L. Birnbaumer, and V. Flockerzi.** 2002. The TRP channels, a remarkably functional family. Cell **108:**595–598.
23. **Okada, T., R. Inoue, K. Yamazaki, T. Kurosaki, T. Yamakuni, I. Tanaka, S. Shimizu, K. Ikenaka, K. Imoto, and Y. Mori.** 1999. Molecular and functional characterization of a novel mouse transient receptor potential protein homologue TRP7. Ca^{2+}-permeable cation channel that is constitutively activated and enhanced by stimulation of G protein-coupled receptor. J. Biol. Chem. **274:**27359–27370.
24. **Porter, V. A., A. D. Bonev, H. J. Knot, T. J. Heppner, A. S. Stevenson, T. Kleppisch, W. J. Lederer, and M. T. Nelson.** 1998. Frequency modulation of Ca^{2+} sparks is involved in regulation of arterial diameter by cyclic nucleotides. Am. J. Physiol. Cell Physiol. **274:**C1346–C1355.
25. **Reynolds, A., D. Leake, Q. Boese, S. Scaringe, W. S. Marshall, and A. Khvorova.** 2004. Rational siRNA design for RNA interference. Nat. Biotechnol. **22:**326–330.
26. **Schilling, W. P.** 2001. TRP proteins. Novel therapeutic targets for regional blood pressure control? Circ. Res. **88:**256–259.
27. **Strübing, C., G. Krapivinski, L. Krapivinski, and D. E. Clapham.** 2001. TRPC1 and TRPC5 form a novel cation channel in mammalian brain. Neuron **29:**645–655.
28. **Trebak, M., G. Vazquez, G. S. Bird, and J. W. Putney, Jr.** 2003. The TRPC3/6/7 subfamily of cation channels. Cell Calcium **33:**451–461.
29. **Welsh, D. G., A. D. Morielli, M. T. Nelson, and J. E. Brayden.** 2002. Transient receptor potential channels regulate myogenic tone of resistance arteries. Circ. Res. **90:**248–250.
30. **Xu, X. Z., F. Chien, A. Butler, L. Salkoff, and C. Montell.** 2000. TRPγ, a drosophila TRP-related subunit, forms a regulated cation channel with TRPL. Neuron **26:**647–657.
31. **Yu, Y., I. Fantozzi, C. V. Remillard, J. W. Landsberg, N. Kunichika, O. Platoshyn, D. D. Tigno, P. A. Thistlethwaite, L. J. Rubin, and J. X.-J. Yuan.** 2004. Enhanced expression of transient receptor potential channels in idiopathic pulmonary arterial hypertension. Proc. Natl. Acad. Sci. USA **101:**13861–13866.
32. **Zhu, X., M. Jiang, M. Peyton, G. Boulay, R. Hurst, E. Stefani, and L. Birnbaumer.** 1996. trp, a novel mammalian gene family essential for agonist-activated capacitative Ca^{2+} entry. Cell **85:**661–671.
33. **Zhu, X., M. Jiang, and L. Birnbaumer.** 1998. Receptor-activated Ca^{2+} influx via human Trp3 stably expressed in human embryonic kidney (HEK)293 cells. Evidence for a non-capacitative Ca^{2+} entry. J. Biol. Chem. **273:**133–142.